SAE INTERNATIONAL®

# Cumulated Microslip in Component Assembly of Engine and Gearbox

2015-01-1737
Published 04/14/2015

**Jean-louis Ligier, Mathieu Benoit, and Sylvain Damaz**
Institut COMATEC

**CITATION:** Ligier, J., Benoit, M., and Damaz, S., "Cumulated Microslip in Component Assembly of Engine and Gearbox," SAE Technical Paper 2015-01-1737, 2015, doi:10.4271/2015-01-1737.



## Abstract

Today new automotive engine design is optimized in terms of mass. However, in terms of structural stiffness, optimizations mainly consider eigenfrequency criteria. But in assembly components with very low stiffness, cumulated microslip phenomena can occur when the structures are subject to cyclic loadings. In time and after a large number of cycles, macro-displacements can be observed between assembly components and then assembly failures will occur. Bush, plain bearing, roller bearing in conrod or in gearbox can be subject to this kind of problem.

In this paper, after a short description of various mechanisms which can cause microreptation phenomena, two types of cumulated microslip occurring in the engine and the gearbox are presented. Behavior specificities will be highlighted to remind how unusual cumulated microslips are. Based on field data, it appears that the probability of both phenomena occurring is extremely low. This implies that it is not appropriate to use devices concerned by this problem in order to reproduce and to investigate the phenomenon. Moreover, to assess the phenomenon sensitivity with respect to certain parameters, it follows that specific test rigs have to be developed. To cope with the problem for gearbox and conrod, two specific test rigs have been designed and finalized. Their schematic description will allow to assess the delicate points of the tests.

Some results obtained on test rigs are detailed and demonstrate that the mechanical behavior of cumulated microslip is quite complex. Friction phenomena in interface assembly appear to be a key characteristic. For example, significant friction variations with respect to time and slip displacement have been observed.

## Introduction

Over the past ten years, automotive engines have undergone major changes. The main evolutions relative to mechanical running conditions for crank train components are:

- The combustion gas pressure increase, particularly for turbocharged diesel engines. Today, it is also true for turbocharged gasoline engines which are increasingly produced on the European market.
- The mass reduction of all engines for cost reduction purposes of automobiles in use. The two main factors are pollutant emission reduction and raw material consumption reduction.
- Engine designs are undergoing downsizing and downspeeding.

Due to these evolutions the engine assembly components can be subject to high deformation as soon as the engine is operating at full load or high speed. Consequently, for designers, it is necessary to take into account the specific behavior of the highly strained components in the engine. With respect to the standard mechanical analysis and for these components during the design period, it is usual to check:

- The internal stresses for several load conditions during the combustion cycle,
- The strain energy during a loading cycle,
- The natural frequency of the component with its specific boundary,
- The maximal elastic displacement.

This information allows the designer to control the quality of the product with respect to fatigue risk, critical vibrations and contact with other parts caused by excessive elastic displacement. But currently two risks are not being investigated. For highly strained engine components, fretting and microslip can occur and induce engine breakage. During the engine design stage, the fretting behavior is rarely considered. Only a few authors have described mechanical analysis with respect to this risk [1, 2, 3]. Even more rare are the papers or design analysis dealing with the risk of cumulative microslip between two assembled components [4-5]. This lack of consideration is mainly due to the small number of registered cases for the engines developed in mass production in the twentieth century. However, this kind of problem, cumulated microslip, has been well known by the racing engine designers and very large diesel engine designers for

many years. Today under the more severe running conditions, this problem can occur on mass production engines as well. The more current problems are related to rotation or translation of small end bush, rotation of conrod bearing, rotation or translation of main bearing and bush translation of secondary gearbox shaft or roller bearing bush fitted in crankcase as described in Figure 1.

The necessity to treat cumulated microslip phenomena is due to the fact that accumulation of micro-displacement at each loading cycle can lead to engine breakdown. To illustrate this point, it is interesting to remind that for highly turbocharged diesel engines, a translation of the small end bush with respect to the conrod is sometimes observed. For approximately 0.5 millimeters of bush translation, contact between the bush and the piston will occur. This contact will lead to bush seizure.

In addition, for conrod bearing or main bearing in gasoline and diesel engines with rotational micro-displacements, seizure can occur. This failure is caused by the unfortunate location of the joint face relief in the loaded area of the bearing. In this case, the joint face relief constitutes a groove which drastically reduces the minimum oil film thickness. Due to the smallness of this film, contact and then seizure occur between the bearing and the shaft.

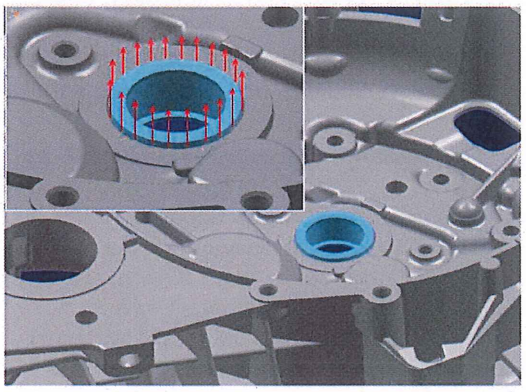

Figure 1. Roller bearing bush translation from crankcase

For modern engines, the cumulative microslip phenomenon has to be considered in order to guarantee reliable engine design. To achieve this task, it is important to have physical explanations of the phenomenon and to have suitable test rigs, due to the lack of documentation and experience on the subject. Then test rigs will allow to assess:

- Firstly, the application specificities,
- Secondly, the sensitivity of assembly components with respect to unavoidable manufacturing dispersion.

At the moment, the best way to apprehend this subject is to jointly use analytical modelling with the "strength of material" and experimental results obtained on test rigs. Strength of material modelling allows us to focus on the mechanical phenomenon by using simple relationships. For example, it can be shown that friction coefficient is one of the key parameters with regard to the occurrence of the phenomenon. The more accurate the friction description is, the more precise the prediction of the occurrence will be. At this stage it is important to emphasize the difficulty to introduce, in refined numerical technique, the correct "ingredients" which allow to reproduce the phenomenon. For example, with the current elasto-hydrodynamic lubrication codes, it is not possible to reproduce that phenomenon. The first reason is related to the lack of unilateral contact between finite solid elements in elasto-hydro-dynamic codes. The second reason is that the numerical model cannot take into account all friction modelling refinements necessary to reproduce realistic cumulated microslips.

From this quick overview it appears necessary to go more in detail about cumulative microslips. Therefore, the next chapters will present:

- the basic mechanics,
- current type of behavior : translation and rotation,
- some tools to model the mechanical behavior,
- specific test rigs which allow to reproduce the phenomenon.

## Basic Mechanisms

Several works [6, 7, 8] have investigated cumulative microslip phenomena and set up the first rules governing them. It appears that some of the necessary conditions (but not sufficient to produce the phenomenon on their own) are:

- the internal shear stress must be higher than the adherence stress for a large area of the interface of the assembly components concerned by cyclic loadings. In mathematical terms, we must verify that:

$$\tau(\partial\Omega) > \mu_{ad} P_{con} \qquad (1)$$

With $\tau$ internal shear stress $\partial\Omega$ the interface, $\mu_{ad}$ adherence coefficient, $P_{con}$ nominal contact pressure.

From a practical point of view, this situation occurs when two parts are pressed together as represented on Figure 2.

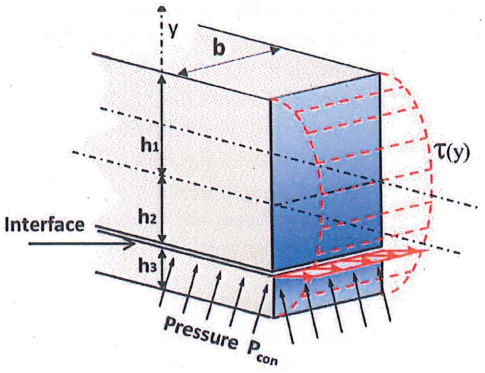


Figure 2. Shear stress at the interface

The current way to produce this internal shear stress is to apply a bending moment due to shear loading to assembly components as it could happen for a bearing shell in its housing (cf. Figure 3). Contact pressure is due to the fitting conditions and the bending moment is due to conrod loading. When slip occurs at the interface, point A undergoes strains in both directions, which are the 'heart' of the micro-displacement.

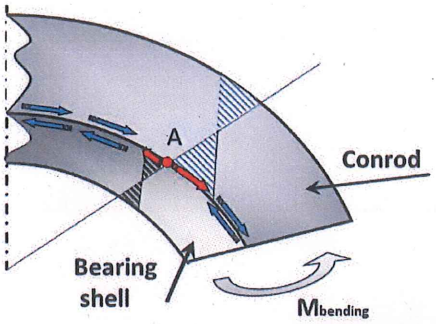


Figure 3. Shear stress between bearing and housing

- Another important condition is that slip does not occur at the same time everywhere on the whole interface. This global slip occurs when Coulomb friction law is used in simulations. One of the solutions consists in using regularized friction law as described in Figure 4.

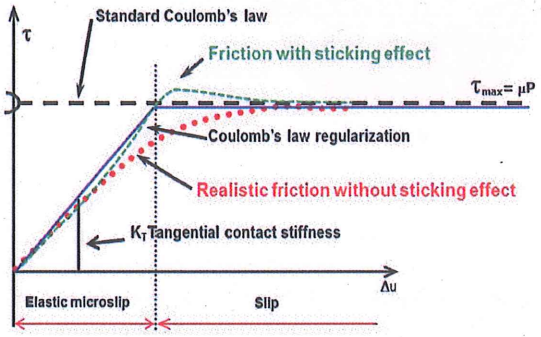


Figure 4. Regularized Coulomb friction law

This regularization is obtained by introducing a micro-elastic displacement before the slip. In a way it represents a bristle behavior [9]. For certain applications, this kind of model is called bristle friction. To take into account some sticking effect when assembly components are immobile, it is possible to consider that static and cinematic friction coefficients are different. The micro-elastic displacement is very important because the elementary global displacement at each loading cycle is proportional to this micro-displacement. From practical considerations on bearing and bush subject to the phenomenon, the elastic microslip varies between 0.05 µm up to 0.3 µm. With structural finite element code, contact simulation involving friction is implicitly done with regularized friction law but the user has to incorporate realistic values of elastic micro-displacement.

- To complete the friction law, it is also necessary to adopt special friction behavior in order to obtain a realistic prediction. The more current friction specificities are related to the dependence of the friction to the displacement, the speed, the time of sticking, the roughness and the interface pollution before the bush fit. To determine which refinement of the friction law must be used, it is quite convenient to proceed with a friction test. For example, the test could simply consist in removing a bush from its housing where it has been fitted as described in Figure 5.

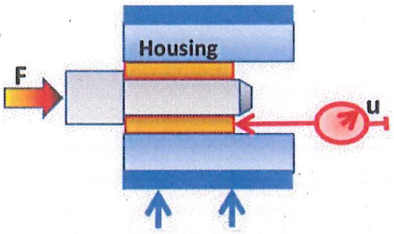


Figure 5. Friction test

- The influence of displacement $u$ from work done by Ferrero and Barrau [10] provides an empirical relationship which correlates quite well with experimentation.

$$\mu(u) = \mu_\infty + (\mu_0 - \mu_\infty)e^{-au} \quad (2)$$

With $u$ displacement, $\mu_0$ the initial friction coefficient, $\mu_\infty$ asymptotic friction coefficient, $a$ parameter.

For certain materials, just 1 or 2 mm suffice to obtain a stabilized friction coefficient and a variation of factor 2 on the friction coefficient. In certain assembly component situations, this characterization could be very useful to assess the cumulative micro-displacement risk. If friction between components increases with displacement, the microslip phenomenon will stop.

- For the influence of very low speed, Berthoud and Baumberger [11] propose the following law which has also given good results:

$$\mu(v) = \mu_0 + \mu_v \ln\left(\frac{v}{v_{ref}}\right) \quad \text{for } v < 20\ \mu\text{m/s} \quad (3)$$

With $v$ velocity, $v_{ref}$ reference velocity, $\mu_v$ the stabilized friction coefficient at high velocity.

- The rest time is also very important but is strongly dependent on the tribological couple in contact. Some authors propose the following expression which has to be confirmed for each given application:

$$\mu(t_r) = \mu_{t\infty} - (\mu_{t\infty} - \mu_0)e^{-\alpha t_r} \quad (4)$$

With $t_r$ rest time, $\mu_{t\infty}$ the stabilized friction coefficient after a long rest time.

- The final necessary condition is the presence of a certain dissymmetry [4,7]. This dissymmetry could be due by the loading, the housing stiffness (the main root cause) and the friction coefficient. For example a flexible conrod with oblique cut naturally undergoes the phenomenon due to its lack of symmetrical housing stiffness.

Taking into account all the previous conditions, the phenomenon can be simulated with more realistic mechanical behavior. For example, regularized friction law has been shown to be a key element in the cumulated microslip simulation [8]. For low tangential stiffness the phenomena can disappear.

## Two Types of Behavior

In this chapter the idea is to present two types of behavior of micro-displacement in assembly components. Quite obvious global micro-displacements could be obtained when certain areas in the contact interface are no longer in contact [12] during the loading of the assembly. But to emphasize the complexity of the phenomenon which is analyzed here, it is interesting to know that the cumulative micro-displacements happen without losing contact pressure between the assembly components. To treat this subject, two examples issued from engine and gearbox are depicted hereafter.

### *Translation Micro-Displacement*

The first behavior we consider is the translation of the fitted component of the assembly. For example in Figure 6, the translation of a bush on a gearbox shaft is investigated. The shaft is in rotation and a very uniform loading is applied on the shaft. For low contact pressure and low friction coefficient, it has been observed some important translation of the bush which supports the roller bearing reaction to the shaft loading.

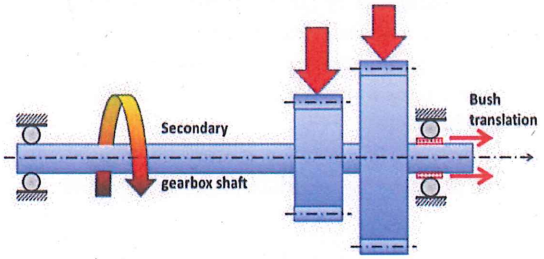


Figure 6. Secondary gearbox shaft

To assess the translation phenomenon it is necessary to consider the loading on this component. In our first approach, we can suppose that the loading on the external part of the bush is distributed parabolically along the horizontal axis and according to a sine law in the circumferential direction (cf. Figure 7 and Figure 8).

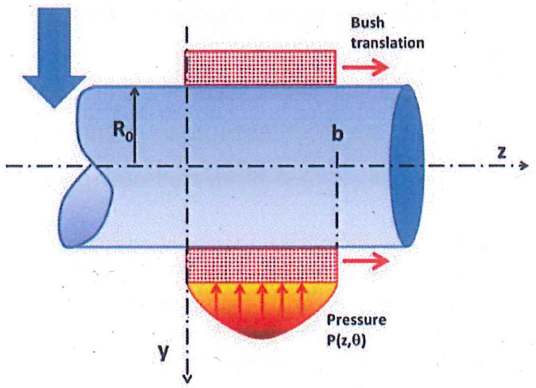


Figure 7. Parabolic distribution

These hypotheses involve the contact pressure field of the roller bearing against the external surface of the bush, which can be described by:

$$P_{rb}=\begin{cases} P_{00}\left(\frac{z}{b}\left(1-\frac{z}{b}\right)\right)\cos(\theta) & for \quad \frac{\pi}{2}<\theta<\frac{3\pi}{2} \\ 0 & for \quad -\frac{\pi}{2}<\theta<\frac{\pi}{2} \end{cases} \tag{5}$$

With $P_{00}=3R_b/R_0b$ and $R_b$ bearing reaction on the bush, b bearing width, $R_0$ shaft radius.

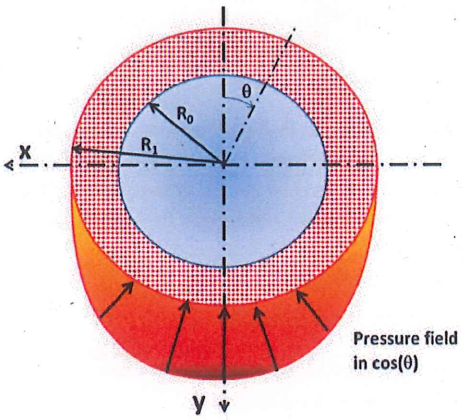


Figure 8. Sinusoidal distribution

From this external loading, the internal contact pressure at the interface between the bush and the shaft must be determined. The initial fitting pressure is presumed to be quite large to avoid any loss of contact at the interface and is called $P_{fr}$. The contact pressure variation along the circumference can be approached by the following relationship. This expression is obtained from elasticity consideration and is detailed in the Appendix.

$$\Delta P=\begin{cases} \frac{-R_1}{R_0}.P_0.\cos(\theta) & for \quad \frac{\pi}{2}<\theta<\frac{3.\pi}{2} \\ \frac{4.(R_0-R_1).P_0}{\pi.(R_0+R_1)}.\left(\nu^*+\frac{(R_1-R_0)}{(R_0+R_1)}\right) & for -\frac{\pi}{2}<\theta<\frac{\pi}{2} \end{cases} \tag{6}$$

With

$$P_0=\frac{1}{b}\int_0^b P_{00}\left(\frac{z}{b}\left(1-\frac{z}{b}\right)\right)dz=\frac{P_{00}}{6} \tag{7}$$

At the end of the gearbox shaft, the shear load generating bending moment, called $T(z)$, is described by the following expression given in the set of axes in Figure 7:

$$T(z)=R_b-R_1\int_0^z P_{00}\left(\frac{\zeta}{b}\left(1-\frac{\zeta}{b}\right)\right)d\zeta \tag{8}$$

This shear load generates, in polar coordinates, some shear stress $\tau_{zr}$ in the assembly bush and shaft:

$$\tau_{zr}(r) = \frac{T(z).(R_1^2.(3+2\nu).\cos(\theta)-(3+2\nu).r^2.\cos^3(\theta))}{\pi.R_1^4} - \frac{T(z)(-3.r^2.\sin^2(\theta).\cos(\theta))}{\pi.R_1^4} \quad (9)$$

To detect the slipping area we have to use the condition:

$$\tau_{zr}(R_0) > f.(P_{fr} + \Delta P) \quad (10)$$

With $f$ being the friction coefficient. But to get accurate results it is interesting to consider static and cinematic friction coefficient. Due to shaft rotation, the slipping area becomes, after a certain rotation angle, an adherent area and so on. But for the transition between the two, the friction coefficient is not the same. The change from adherent area to slipping adherent needs static friction coefficient instead cinematic friction coefficient for the inverse change.

After application of the previous inequality (10), the slipping area can be determined. The shape of this area could be those in Figure 9.

By taking into account the worst conditions due to the manufacturing process, it is possible to check if cumulated micro-slips will happen. The phenomenon occurs when the slipping area is greater than a certain threshold. This threshold needs to be deduced through experimentation. Test rigs where all parameters are well known and under control will fully contribute to this analysis and to identify this threshold. Such test rigs will be described in the next chapter.

From a practical point of view the current solutions to postpone the phenomenon with respect to the loading are:

- to increase the fitting pressure,
- to reduce the loading as much as possible,
- to increase the stiffness or to make it more symmetrical,
- to increase the friction coefficient,
- to reduce the tangential contact stiffness at the interface, for example by increasing the roughness, contrary to common sense.

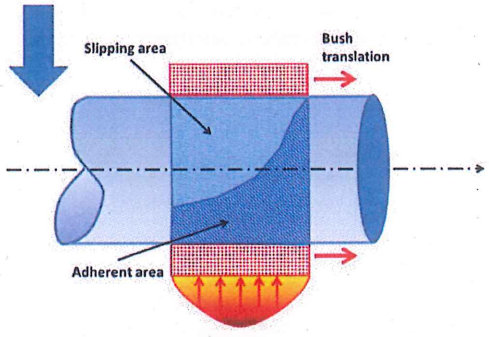


Figure 9. Slipping area in the interface

## *Rotation Micro-Displacement*

The second type of behavior is more often mentioned in documentation and is related to the bush or bearing rotation. The example analyzed in this paper is the small end bush of the engine conrod. To generate cumulative microslip between the bush and its housing, special conditions are necessary. The small end must be subject to axial loading combined with lateral loading in order for the rotation to potentially happen. The lateral loading comes from a high regime and a large rotational inertia of the conrod with respect to its gravity center. This loading represents the condition of a non-symmetrical situation for the small end. Under these hypotheses the bush can rotate.

As the small end of the conrod has lubrication holes and sometimes joint face or has trapezoidal shape (viper head), after a certain number of cycles, it can happen that these features are located in a bad area for the bush lubrication. Then bush seizure could occur. For the small end the worst loading producing slip at the bush interface is the inertia loading as represented in Figure 10. In that case the housing is very flexible with respect to the loading direction and a wrapping effect of the housing around the piston pin can often be observed. The semi wrapping angle can reach values close to 90° [14]. Outside this wrapping angle, the curvature variation of the small end is produced by a no pure bending moment. This generates internal shear stress in the assembly and the previous condition, particularly condition (1), could be expected to produce a cumulative microslip phenomenon.

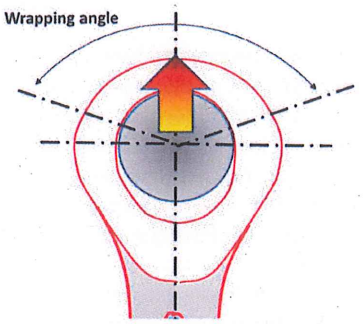


Figure 10. Inertia loading on small end

The consequence of this wrapping is a special pressure contact distribution between the pin and the bus as represented in Figure 11 [14]. This kind of pressure is well known and corresponds to a non hertzian contact. In this figure two types of normal stresses are plotted to represent the link between the small and the conrod shank for two conrod types. The lateral loading will give a not perfectly symmetrical shape with respect to the conrod axis.

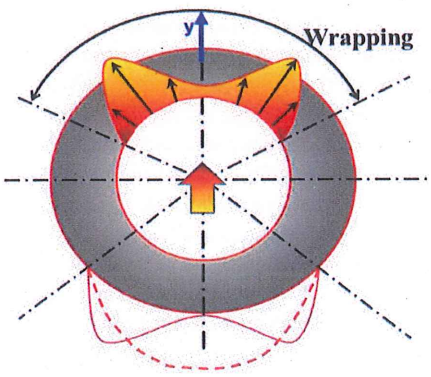


Figure 11. Zoom and contact pressure of small end

At the stage, it is possible to use the strength of material theory to model the displacement between the bush and its housing. One way to obtain this modeling is to suppose that the small end housing is concentrated on its average line and behaves like a Timoshenko beam. These hypotheses intend to solve the following equation related to a circular Timoshenko beam.

$$\frac{d^2u_r(\theta)}{d\theta^2}+u_r(\theta)=-\frac{R_m^2}{EI_{fo}}M_f(\theta) \quad \text{and} \quad \frac{du_\theta(\theta)}{d\theta}-u_r(\theta)=\frac{R}{ES}N(\theta) \tag{11}$$

With $u_r$ the radial displacement of the housing, $u_\theta$ the circumferential displacement, $M_f$ the bending moment and $N$ the normal loading. Analytical solutions can be obtained but, for simplicity purposes, they are not mentioned here because they are quite long (at least 4 to 6 lines of equations). With formal calculation codes, a solution is easy to obtain and easy to handle.

The elongation of the housing, noted $\Delta C_{irL}$, is evaluated by the relationship:

$$\Delta C_{irL}=\int_{\psi}^{2\pi-\psi}\varepsilon_{\theta\theta}Rd\alpha=\int_{\psi}^{2\pi-\psi}\left(\frac{u_r}{R}+\frac{du_\theta}{Rd\alpha}\right)Rd\alpha \tag{12}$$

This elongation will modify the fitting pressure of the bush. But the piston pin loading changes interface pressure distribution. In loading direction, interface pressure increases and in the opposite direction contact pressure decreases. Considering the bush as a circular beam with no bending stiffness, it is possible to evaluate if this beam slips or not with respect to the housing. From these results we can determine the interface area ratio where condition (1) is respected.

With similar reasoning, criterion based on slipping area ratio can be set up to identify occurring conditions for cumulative microslips. From a practical point of view, it has been calculated that for very low friction coefficient the phenomena can occur under normal running engine conditions. This means that it is not necessarily the case that the inertia loading, producing some contact loss in the bush interface, will be applied on the conrod. Generally this loading is around 3 or 4 times higher than the inertia loading in the engine at full speed [12].

## Test Rig for Bush Translation

In order to confirm the accuracy of the previous modelling related to bush translation motion and in certain cases to determine some correlation parameters, a special test rig has been developed. Some adaptations have been made on an old fatigue test rig [15]. On the right side of Figure 12, there is a rotating mandrel with a shaft on which a bush is fitted. On the left side of the figure there is a special device with cam to apply a calibrated load on the bush. Load and speed can vary from 0 to an equivalent situation of the bush on the gearbox shaft when the first speed is engaged.

Before starting the test rig the shaft with the bush are presented in Figure 13. The shaft and the bush dimensions are obtained from similitude considerations with the gearbox problem. An optical gage allows to determine the condition initiating the cumulative microslip phenomenon.

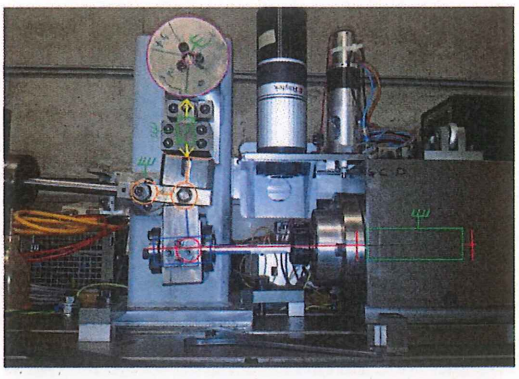

Figure 12. Test rig producing bush translation

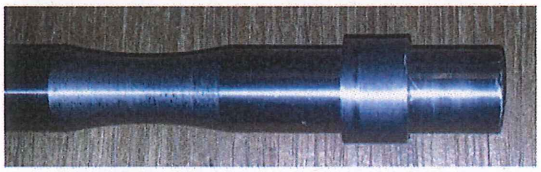

Figure 13. Bush before test

After the test, the bush has moved in translation with no relative rotational displacement (cf. Figure 14). The translation displacement is quite important after 10000 revolutions. The delicate point is to initiate the translation. It has been observed that for certain situations, several hours could be necessary to start the translation. It seems that this time reduces the sticking effect at the interface.

Figure 14. Bush after more than 10000 revolutions.

From this test rig it has been possible to test some sensitivity parameters as the fitted pressure (cf. Figure 15), the shaft roughness, the loading and the initiating time. For these sensitivity analyses it appears obvious from experimental results that friction has a very complex behavior. Friction refinements, previously mentioned, need to be taken into consideration to get realistic simulation predictions.

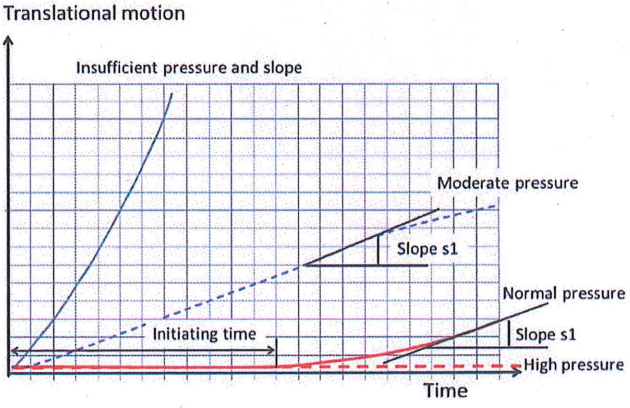


Figure 15. Fitting pressure sensitivity

In Figure 15, four behavior types are illustrated. For very low fitting pressure the bush can slip too easily. In this specific case, beam slope contributes mainly to translation motion. Rotational motion can be observed. Above a certain fitting, pressure translation seems to occur with a very constant speed corresponding to approximately to 0.05 to 0.5 µm per revolution. It has also been noted that for certain pressures, an initiating time delays the occurrence of the phenomenon. But for high pressure no slip has been found. The qualifiers low, moderate, high are related to the slipping area proportion in bush interface.

## Test Rig for Small End Bush Rotation

For small end, the test rig must operate similarly to the loading of a conrod in an engine, which is a big challenge. The way chosen has been to do the loading with an eccentric device. Axial and lateral load can be applied independently on the conrod as illustrated in Figure 16. The various loadings can vary as sine law with respect to time. It is possible to get reciprocating or corrugated loadings with adjustable magnitude for longitudinal and lateral loadings.

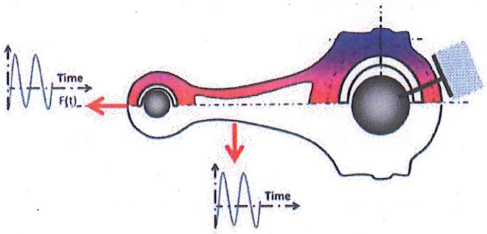


Figure 16. Conrod loading in test rig

Figure 17 gives an overview of the special device built for this particular application. Maximal load considered is around $8.10^4$ N with low rotational speed. To withstand this loading a box structure has been chosen. The load control is done by strain gages on the flexible part of the structure. In this device, the conrod is located at the left hand of the horizontal slider.

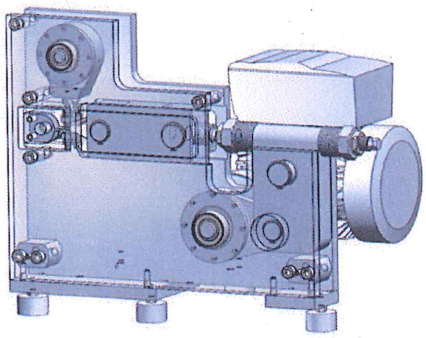

Figure 17. Test rig for small end rotation

A back view of the device is given in Figure 18 where the electric engine and the synchronous belt transmission can be seen.

Figure 18. Back of test rig

An example of loading applied on the conrod is given in Figure 19. This loading with an exaggerated lateral loading with respect to engine loading often produces bush microslip. Some distortions with respect to perfect sine laws are caused by clearance and component elasticity.

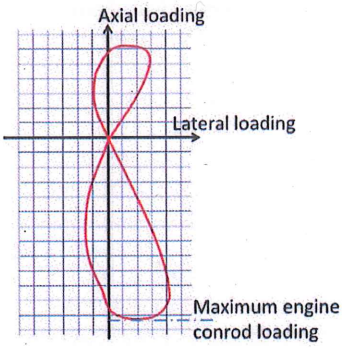


Figure 19. Loading type on test rig

In order to be able to detect the instance where the small end bush begins to rotate, a special instrumentation has been done with 3 strain gages coated simultaneously on the bush face and on the small end face (cf. Figure 20). Obviously the measurement is inaccurate but the initiating conditions are well identified.

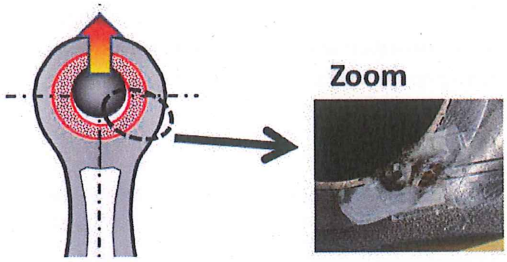


Figure 20. Strain gages between bush and conrod

Figure 21 illustrates an example of a recording from a gage signal related to the loading. When the bush strain gage signal is increasing with respect to time it means that a relative displacement between the bush and its housing is occurring. The initiating time can be clearly seen and the instance where the strain gage is completely debonding from one of the two surfaces.

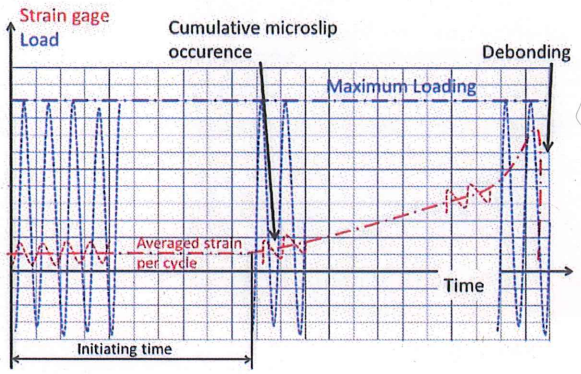


Figure 20. Strain gages recordings

Among the surprising experimental results with small end, maturating time appears necessary to generate the phenomenon as it has been observed on the previous test rig. The slope of displacement against cycles is clearly lower than the previous slope obtained for translation. Also, with certain tribological couples, it has been observed that the rotation could stop after a path of a few mm.

## Conclusions

Despite the poor knowledge about the microslip phenomenon in the car engine industry, cumulated microslips will concern more and more assembly components. This is due to their low stiffness induced by mass optimization. Microslip is more current and known in racing engines or in very large engines such as power plant engines. Microslip mechanism is quite complex and difficult to precisely simulate. It is particularly difficult to determine its exact occurrence with respect to mechanical parameters. Moreover its prediction implies considering complicated friction law which has to be characterized. To be successful in accurate phenomenon prediction it is necessary to couple analytical and experimental investigations. As main microslip displacements are translation and rotation, two test rigs have been developed. With analytical and experimental results it has been possible:

- to predict phenomenon occurrence,
- to confirm that translation or rotation could happen without losing contact pressure between assembly components.

## References

1. Merritt, D. and Zhu, G., "The Prediction of Connecting Rod Fretting and Fretting Initiated Fatigue Fracture," SAE Technical Paper 2004-01-3015, 2004, doi:10.4271/2004-01-3015.
2. Sadwinsli M.P., Farris T.N., Mechanics of Fretting Fatigue Crack Formation. Wear 198. 1996
3. Hupperich P., The Development of the General Electric GEVO Engine, CIMAC Congress, Kyoto (Japan), 2004
4. Antoni N., Phénomène de microreptation des assemblages mécaniques. Thèse de l'Université de Savoie - Chambéry France, Novembre 2005
5. Ligier J.-L., Baron E., Acyclisme et Vibrations. Editions Technip. 2002
6. Antoni N., Nguyen Q.-S, Ligier J.-L., On the cumulative microslip phenomenon. European Journal of Mechanics A/ Solids 26 (2007) 626-646.
7. Antoni N., Ligier J.-L., Asymmetric friction: Modelling and experiments. Int. J. Eng. Sci. 2007.
8. Ligier J.-L., Antoni N., Cumulative microslip in conrod big end bearing system. ASME, May 8-10 2006.
9. Liang J., Fillmore S., Ma O., An extended bristle friction force model with experimental validation. Mechanism and Machine Theory, Volume 56, October 2012, pp 91-100.
10. Ferrero J. F., Barrau J.-J., Study of dry friction under small displacements and near-zero sliding velocity, Wear Vol.: 209, Issue: 1-2, Pages: 322-327, 1991.
11. Berthoud P., Baumberger T., Shear stiffness of a solid-solid Multicontact interface. Proc. R. Soc. Lond. A 454 (1998) 1615-1634.
12. Marmorini L., Baldini A., Bertocchi E., Giacopini M., Rosi R. & al., On the loosening mechanism of a bush press-fitted in the small end of a connecting rod; Proc. IMechE Part D. J. Automobile Engineering. 2011, 226, 312-324.
13. Timoshenko S. P., Goodier J. N., Theory of Elasticity, McGraw-Hill, 3rd ed. 1970.
14. Stievenard A., Ligier J-L., A simplified approach to predict sensitivity factors for the small end conrod of sports car engines, 12th EDF/Pprime Workshop: Futuroscope, October 6 & 7, 2013.
15. Damaz S. Analyse d'un phénomène de microreptation et élaboration d'un banc d'essai dédié. Internal report, Engineering school: Mines de Douai. 2014.

## Contact Information

Additional information can be obtained here:

jean-louis.ligier@heig-vd.ch

HEIG-VD Comatec
1 route de cheseaux
1400 Yverdon-les-bains
Switzerland

# APPENDIX

## Pressure Distribution in the Bush

To perform this analysis, the bush is presumed to have a small ratio L/D. Using St. Venant principle's [10], it is possible to admit that any circumferential stress could be considered as uniform with respect to the axial direction, the width. To perform calculation in plane strain, E and ν are switched, in standard elasticity relationship, by:

$$E^* = \frac{E}{1-\nu^2} \quad and \quad \nu^* = \frac{\nu}{1-\nu}$$

The behavior relationships in polar coordinates become, with cylinder axis *ox* :

$$\varepsilon_r = \frac{1}{E^*}.(\sigma_r - \nu^*.(\sigma_\theta + \sigma_x)) \text{ and } \varepsilon_\theta = \frac{1}{E^*}.(\sigma_\theta - \nu^*.(\sigma_r + \sigma_x))$$

Relationships between strains and displacements are :

$$\varepsilon_r = \frac{\partial u_r}{\partial r} \text{ and } \varepsilon_\theta = \frac{1}{r}.(\frac{\partial u_\theta}{\partial \theta} + u_r)$$

The contact pressure variation is estimated in the upper part of the bush. This variation mainly follows from the elongation of the lower part. The sine load contributes to this elongation by Poisson effect. So, we can write:

$$\varepsilon_r = \frac{-P(\theta)}{E^*} \text{ and } \varepsilon_\theta = \frac{\nu^*.P(\theta)}{E^*}$$

The total displacement of the lower part is estimated on the average line of the bush after integration of the radial strain.

$$u_r = \frac{-P(\theta)}{E^*}.\frac{e}{2}$$

With this expression introduced in the circumferential strain we can get the circumferential displacement after integration on the average line of the bush :

$$u_\theta = \int_0^\pi (\frac{\nu^*.P(\theta)}{E^*}.\frac{R_0+R_1}{2} - u_r).d\theta = \frac{P_0}{E^*}.(\nu^*.(R_0+R_1)+e)$$

The circumferential stress variation in the upper part of the bush is obtained by supposing that this is mainly due to the lower part elongation. So, the variation is:

$$\Delta\sigma = P_0.(\frac{2.\nu^*}{\pi} + \frac{2.e}{\pi.(R_0+R_1)})$$

For thin shell, the pressure variation is:

$$\Delta P = \frac{2.\Delta\sigma.e}{(R_0+R_1)}$$

Contact pressure variation can still be written:

$$\Delta P = \frac{4.e.P_0}{\pi.(R_0+R_1)}.(\nu^* + \frac{e}{(R_0+R_1)})$$

Finally, the variation pressure field between the bush and the housing is defined by:

$$\Delta P = \begin{cases} \frac{-R_1}{R_0}.P_0.\cos(\theta) & for \ \frac{\pi}{2} < \theta < \frac{3.\pi}{2} \\ \frac{-4.e.P_0}{\pi.(R_0+R_1)}.\left(\nu^* + \frac{e}{(R_0+R_1)}\right) & for -\frac{\pi}{2} < \theta < \frac{\pi}{2} \end{cases}$$

The Engineering Meetings Board has approved this paper for publication. It has successfully completed SAE's peer review process under the supervision of the session organizer. The process requires a minimum of three (3) reviews by industry experts.



ISSN 0148-7191

http://papers.sae.org/2015-01-1737